

Supporting information for

Probing water adsorption and stability under steam flow of Zr-based metal-organic framework using ^{91}Zr solid-state NMR spectroscopy

Athulya Nadol^a, Florian Venel^a, Raynald Giovine^a, Maëva Leloire^a, Christophe Volkinger^a, Thierry Loiseau^a, Christel Gervais^b, Caroline Mellot-Draznieks^c, Bertrand Doumert^d, Julien Trébosc^d, Olivier Lafon^a, Frédérique Pourpoint^{*a}

- a. Univ. Lille, CNRS, Centrale Lille, ENSCL, Univ. Artois, UMR 8181 – UCCS – Unité de Catalyse et Chimie du Solide, F-59000 Lille, France
- b. LCMCP, UMR 7475, Sorbonne Université, CNRS, F-75005 Paris, France
- c. Laboratoire de Chimie des Processus Biologiques (LCPB), CNRS UMR 8229, Collège de France, PSL University, Sorbonne Université, Paris 75231, France
- d. IMEC, Univ. Lille, CNRS, Centrale Lille, Univ. Artois, FR 2638, F-59000 Lille, France
- e. Institut Universitaire de France, 1, rue Descartes – 75231 Paris CEDEX 05, France

*Corresponding author: frederique.pourpoint@centralelille.fr

Section	Content	page
Fig. S1	Representation of the atomic-level structures of the three samples	2
Fig. S2	Picture of the experimental set-up to measure and control the steam flow and the temperature	3
Fig. S3	XRD	4
Fig. S4	IR spectra	5
Fig. S5	N_2 adsorption	6
Fig. S6	$^1\text{H} \rightarrow ^{13}\text{C}$ CPMAS NMR spectra	7
Table S1	Zr-O distances expected in the three samples according to the published CIF files	9
Table S2	Number of experimental echoes in the QCPMG	9
Fig. S7	WURST-QCPMG added spectra of UiO-66	10
Fig. S8	WURST-QCPMG added spectra of UiO-66-Fum	11
Fig. S9	WURST-QCPMG added spectra of UiO-67-NH ₂	12
Table S3 Fig. S10	Simulations of ^{91}Zr using regular quadrupolar lineshape	13
Table S4 Fig. S11	Calculated NMR parameters for UiO-66-Fum	14
Table S5 Fig. S12	Calculated NMR parameters for UiO-66-Fum-H ₂ O	15
Table S6 Fig. S13	Calculated NMR parameters for UiO-67-NH ₂	16
Table S7 Fig. S14	Calculated NMR parameters of reference compounds	17
	References	18

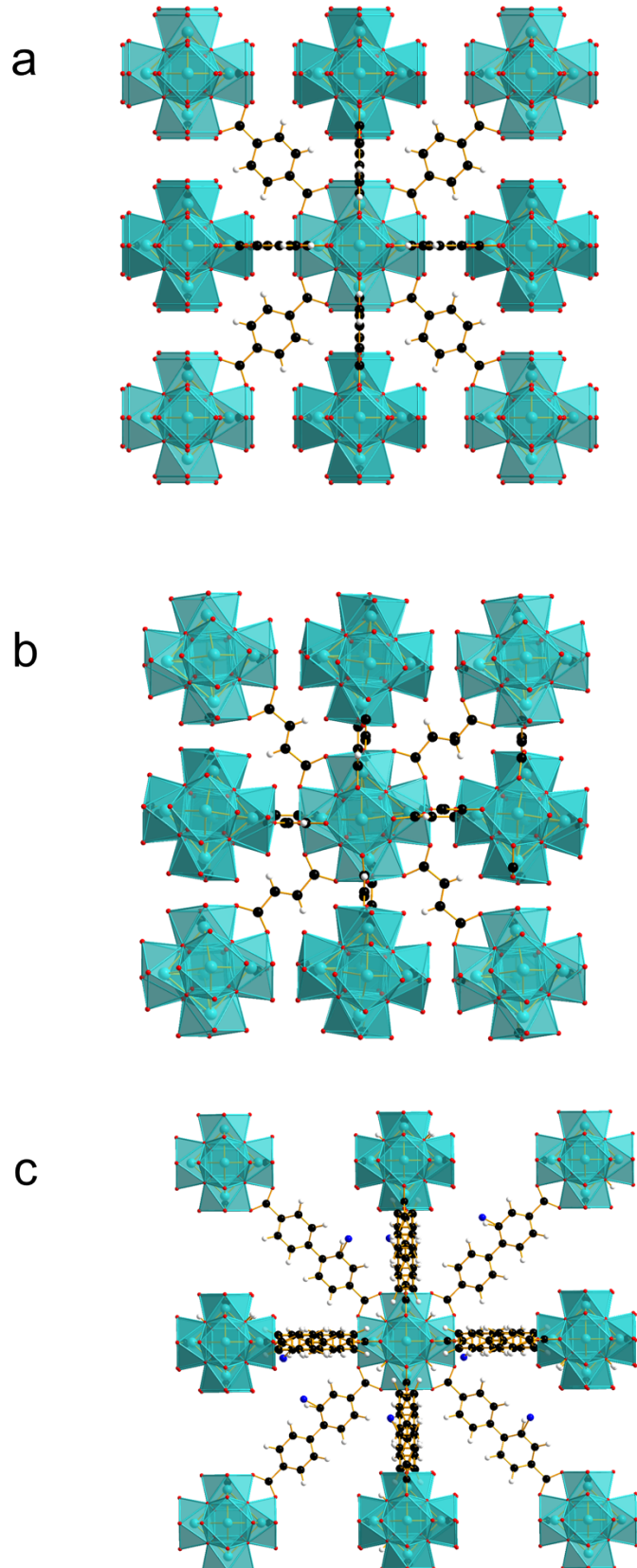


Figure S1. Atomic-level structures of (a) UiO-66^1 , (b) UiO-66-Fum^2 and (c) UiO-67-NH_2^3 determined by X-ray diffraction. The atoms are displayed with the following colors: zirconium in cyan, oxygen in red, carbon in black, nitrogen in blue, and hydrogen in gray. Furthermore, $\text{Zr}_6\text{O}_4(\text{OH})_4$ clusters are displayed as cyan polyhedra.

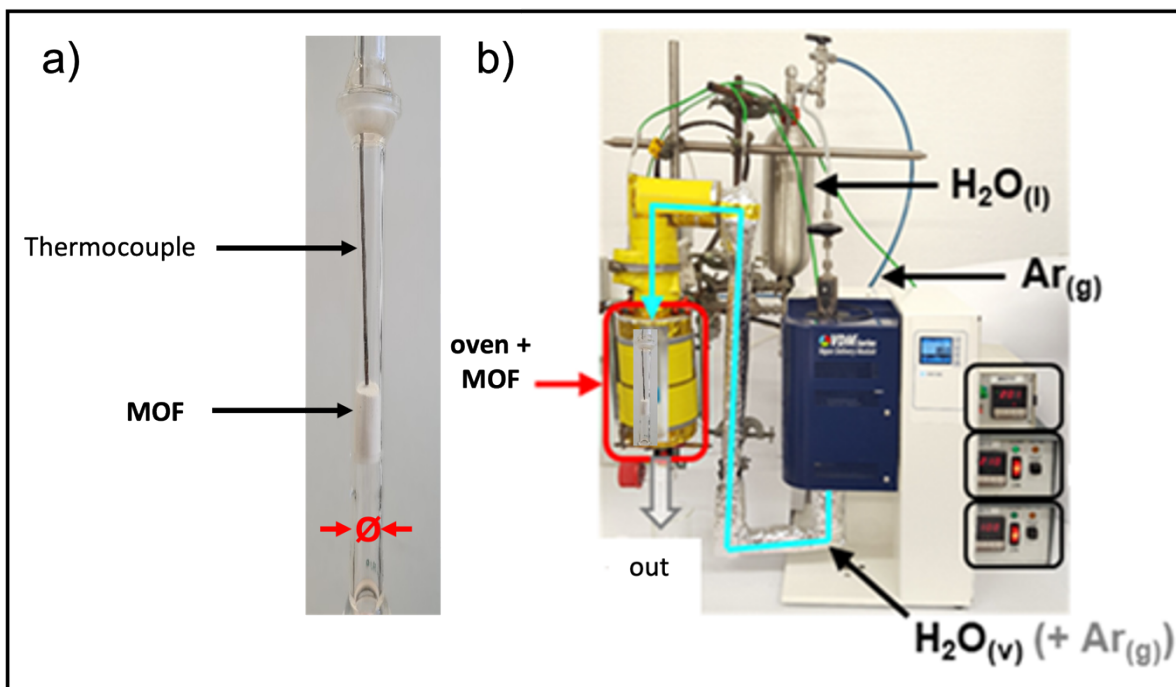


Figure S2. Experimental setup used to study the stability of MOF under steam flow at different temperatures.

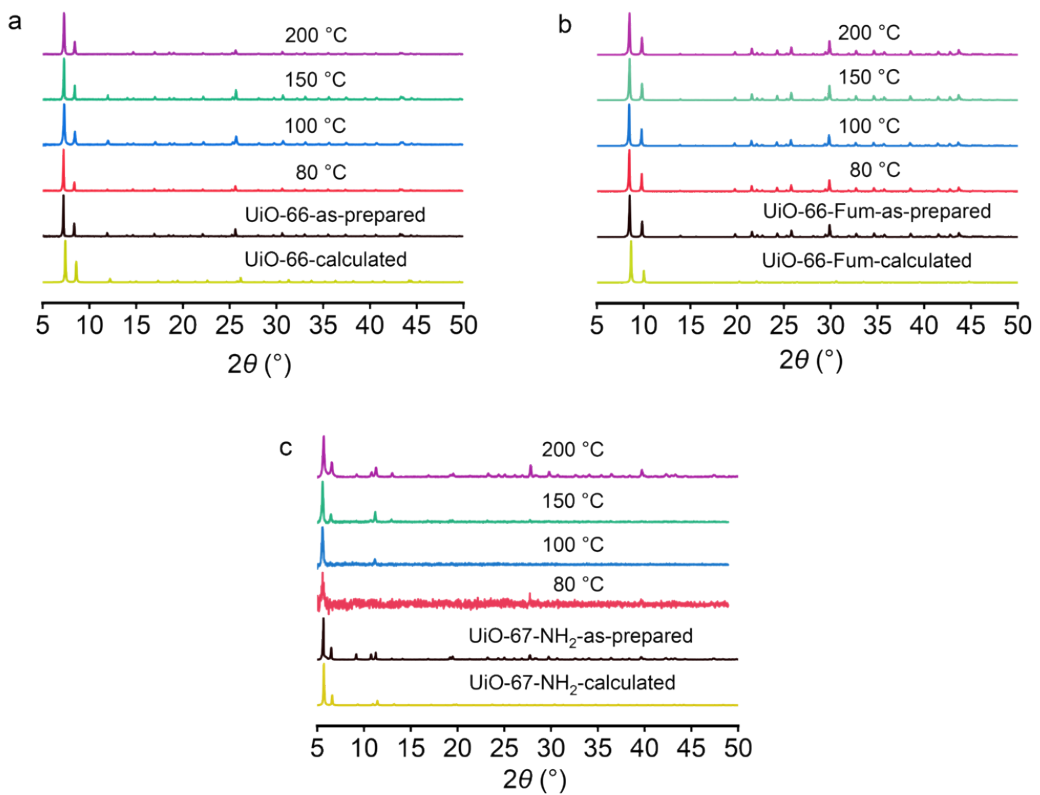


Figure S3. Comparison of experimental XRD patterns for the MOFs (a) UiO-66 , (b) UiO-66-Fum , and (c) UiO-67-NH_2 : calculated from the crystalline structures reported literature, (see ref. 1 for UiO-66 , 2 for UiO-66-Fum and 3 for UiO-67-NH_2) (light green), as-prepared (black) and after steam treatment at 80 (red), 100 (blue), 150 (green) and 200 °C (purple). The water treatment lasted 7 days for UiO-66 and 24 h for UiO-66-Fum and UiO-67-NH_2 .

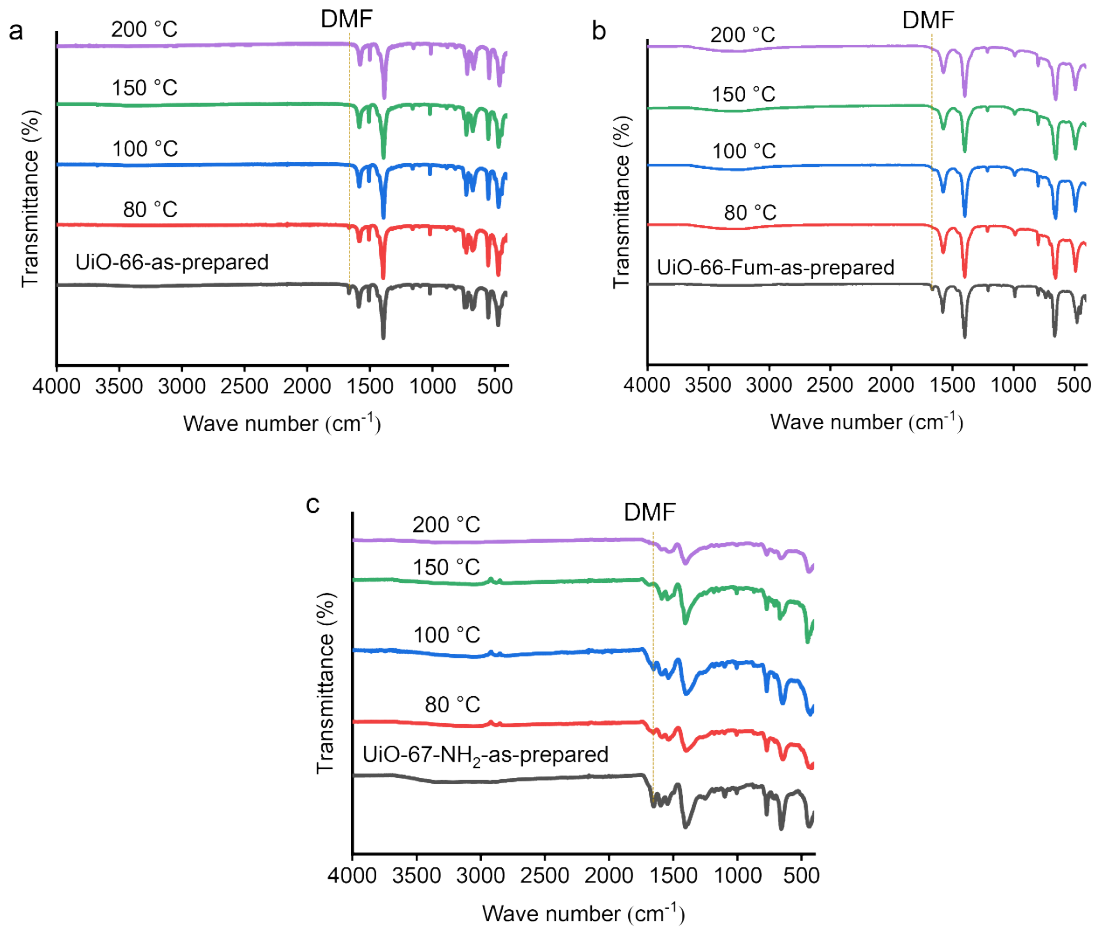


Figure S4. FTIR spectra of the three samples, (a) *UiO-66*, (b) *UiO-66-Fum* and (c) *UiO-67-NH₂*: as prepared (in black), and after steam treatment at 80 (in red), 100 (in blue) 150 (in green) and 200 °C (purple).

For all samples, the O–H stretching band near 3600–3400 cm⁻¹ is broad and difficult to detect because of the adsorption of water and DMF in the pores.⁴ IR spectra of the three MOFs are not significantly modified after the steam flow treatment. The main change for the three compounds is the decrease of the band at 1655 cm⁻¹ assigned to the stretching of C=O bond in DMF. This observation indicates that the DMF molecules used for washing of MOFs and adsorbed in the pores are removed by steam flow treatment.

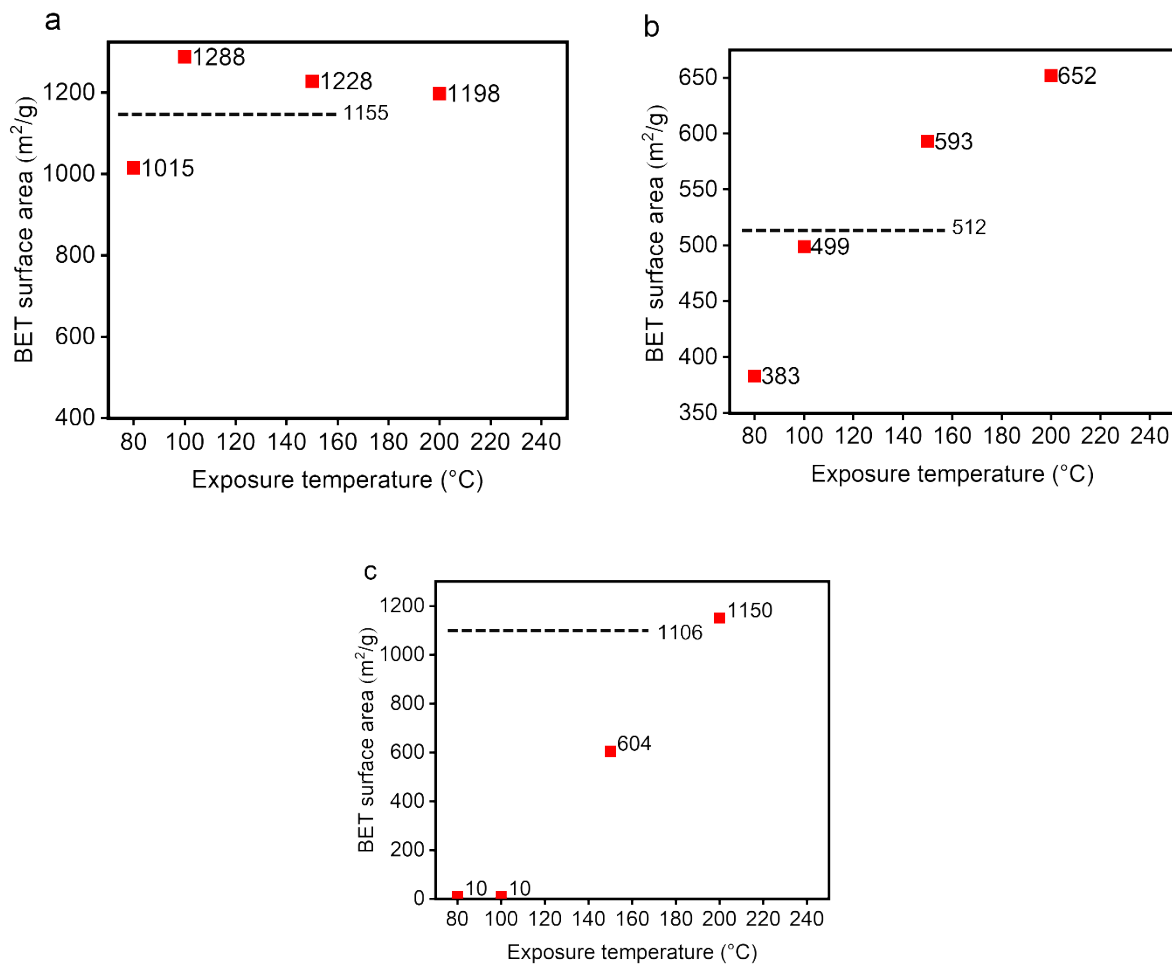


Figure S5. BET surface areas measured for the MOFs (a) UiO-66, (b) UiO-66-Fum and (c) UiO-67-NH₂ submitted to steam flows at temperatures ranging from 80 to 200 °C. The dashed line represents BET surface of the as-prepared sample.

The removal of adsorbed DMF (observed by IR) increases the BET surface areas of UiO-66, UiO-66-Fum and UiO-67-NH₂ treated by steam flows at temperatures greater than or equal to 100, 150 and 200 °C, respectively. Conversely, the treatment at 80 °C slightly reduces the BET surface areas of UiO-66 and UiO-66-Fum, probably owing to the condensation of water in the pores. For UiO-67-NH₂, the BET surface area is significantly reduced at 150 °C and decreases by two orders of magnitude after steam flow treatment at 80 and 100 °C. This substantial drop in surface area indicates the collapse of the porous structure of this MOF when exposed to steam flow at 150 °C or lower.⁵

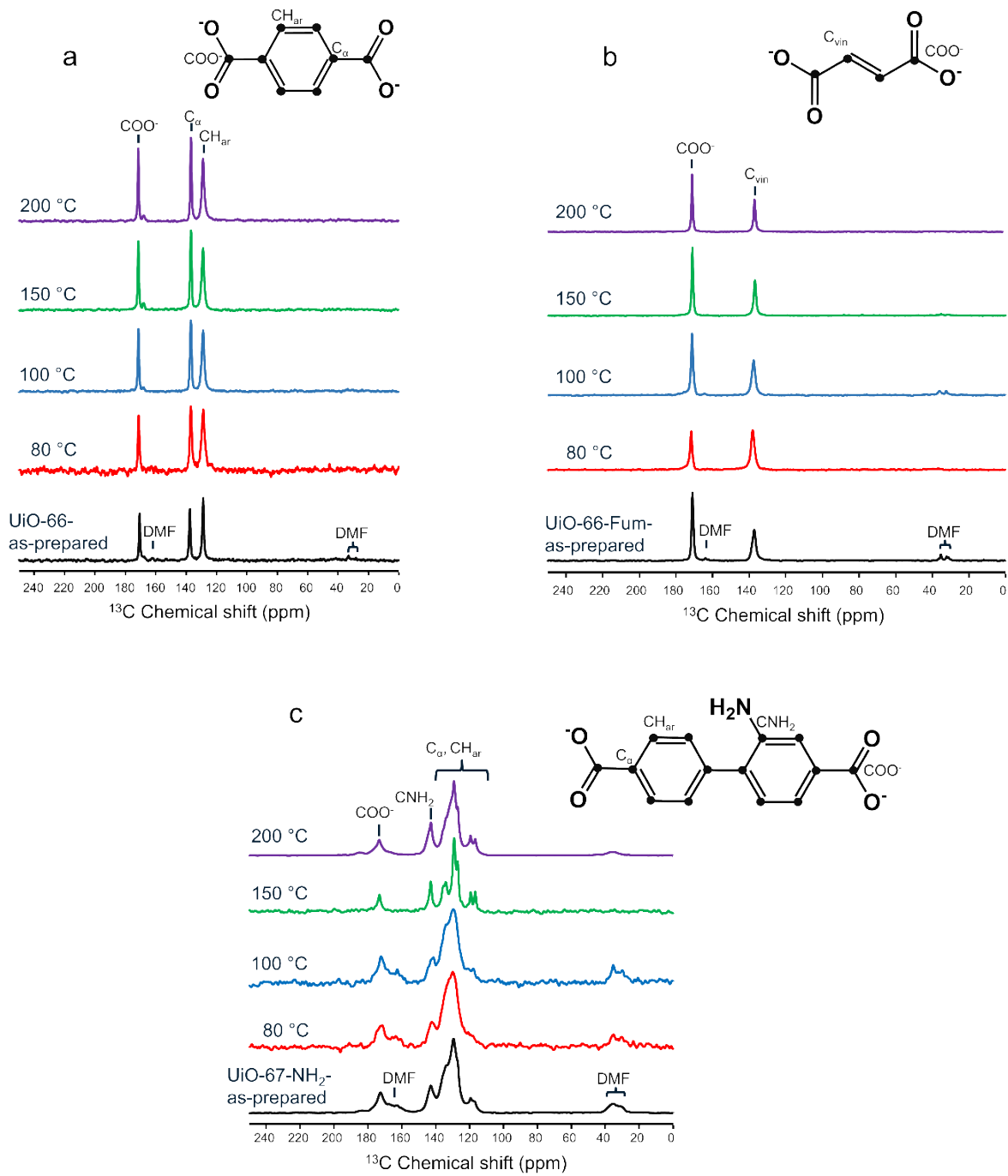


Figure S6. 1D $^1\text{H} \rightarrow ^{13}\text{C}$ CPMAS of (a) UiO-66 , (b) UiO-66-Fum and (c) UiO-67-NH_2 : as-prepared (black) and after steam treatment at 80 (red), 100 (blue), 150 (green) and 200°C (purple).

The 1D $^1\text{H} \rightarrow ^{13}\text{C}$ CPMAS spectra of UiO-66 remain identical before and after steam treatment, which confirms the stability of this MOF under these conditions. We can only notice a drop in the signal-to-noise ratio after the treatment at 80 °C since the condensation of water in the pores accelerates the spin-lattice relaxation of protons in the rotating frame, $T_{1\text{p}}(^1\text{H})$, and hence, reduces the efficiency of the $^1\text{H} \rightarrow ^{13}\text{C}$ polarization transfer. Weak signals of DMF are also visible but they disappear after steam flow treatment.

The 1D $^1\text{H}\rightarrow^{13}\text{C}$ CPMAS spectra of UiO-66-Fum are dominated by the signals of the fumarate linkers. In agreement with ^1H NMR data, signals of DMF (at 32.2, 35.4 and 163.8 ppm) are also visible in the as-prepared sample and those treated by steam flow at temperatures lower than or equal to 100 °C.

The 1D $^1\text{H}\rightarrow^{13}\text{C}$ CPMAS spectra of UiO-67-NH₂ is dominated by the signals of the organic linker. DMF signals are also visible. A slight broadening of the signals appear at 80 and 100 °C, suggesting slight changes on the local environment in contrast with the spectra at 150 and 200 °C. This result leads to the conclusion that the ligand remains roughly intact after the different heat treatment.

Table S1. Zr-O bond distances of the Zr crystallographic site in the reported crystal structures of UiO-66, UiO-66-Fum and UiO-67-NH₂.

Bond distance (Å)	UiO-66 ¹	UiO-66-Fum ²	UiO-67-NH ₂ ³
Zr-O1	2.06	2.06	2.04
Zr-O2	2.06	2.07	2.04
Zr-O3	2.21	2.22	2.18
Zr-O4	2.21	2.22	2.18
Zr-O5	2.25	2.27	2.23
Zr-O6	2.25	2.27	2.23
Zr-O7	2.25	2.27	2.23
Zr-O8	2.25	2.27	2.23

Table S2. Number of detected echoes in the QCPMG experiments.

Sample name	Number of detected echoes
UiO-66-as prepared	50
UiO-66-80 °C	50
UiO-66-100 °C	200
UiO-66-150 °C	200
UiO-66-200 °C	50
UiO-66-Fum-as prepared	200
UiO-66-Fum-80 °C	30
UiO-66-Fum-100 °C	50
UiO-66-Fum-150 °C	200
UiO-66-Fum-200 °C	200
UiO-67-NH ₂ -as prepared	15
UiO-67-NH ₂ -80 °C	2
UiO-67-NH ₂ -100 °C	5
UiO-67-NH ₂ -150 °C	10
UiO-67-NH ₂ -200 °C	10

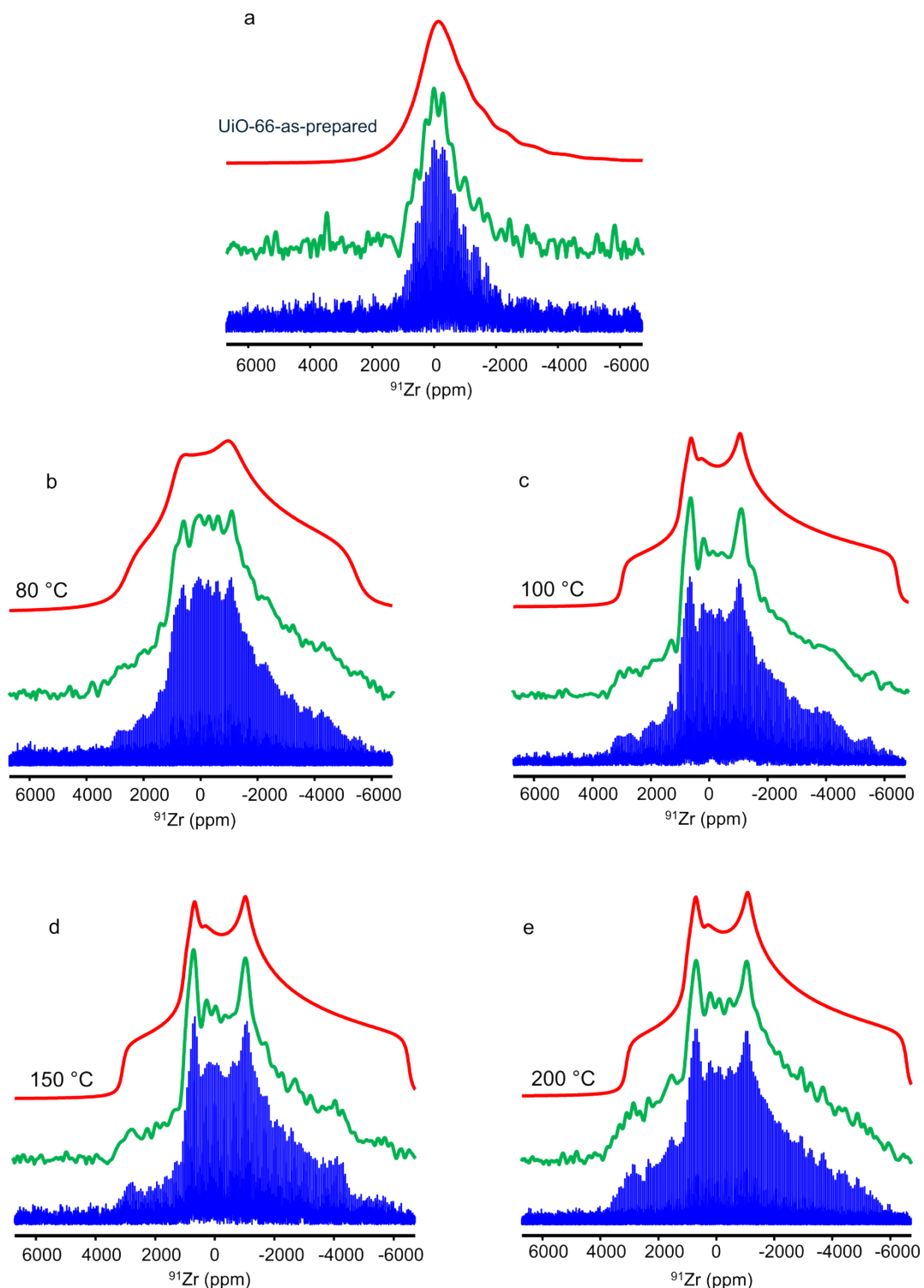


Figure S7. Experimental 1D ${}^{91}\text{Zr}$ WURST-QCPMG NMR spectra of UiO-66: (a) as-prepared or after steam flow treatment at (b) 80, (c) 100, (d) 150 and (e) 200 °C. The spikelet spectra in blue are obtained by the FT of the echo train and are identical to those displayed in Figures 3a and 4, whereas the envelopes in green results from the FT of the sum of the echoes. The red spectra correspond to the simulation using dmfit software.

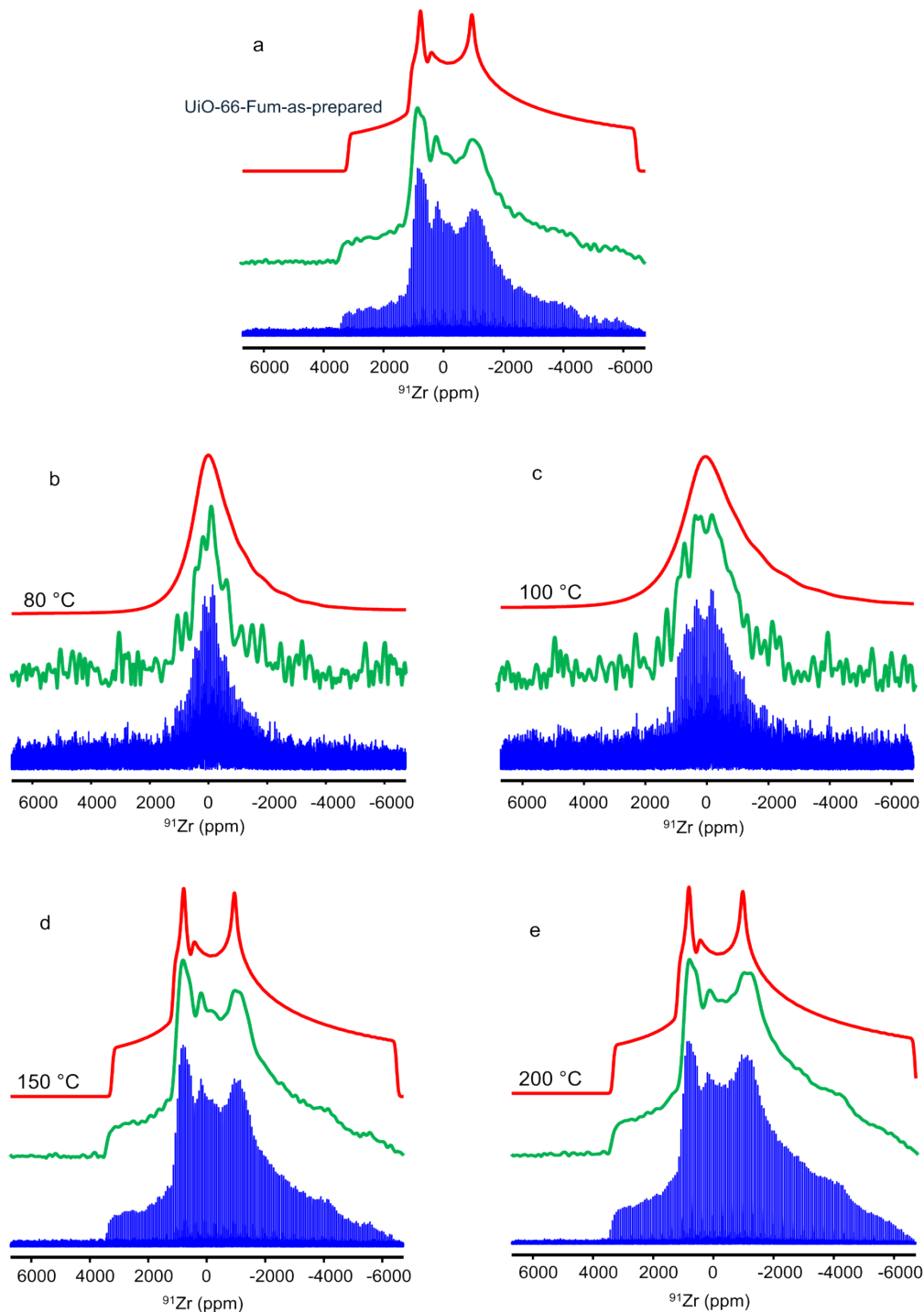


Figure S8. Experimental 1D ${}^{91}\text{Zr}$ WURST-QCPMG NMR spectra of UiO-66-Fum : (a) as-prepared or after steam flow treatment at (b) 80, (c) 100, (d) 150 and (e) 200 °C. The spikelet spectra in blue are obtained by the FT of the echo train and are identical to those displayed in Figures 3b and 5, whereas the envelopes in green results from the FT of the sum of the echoes. The red spectra correspond to the simulation using dmfit software.

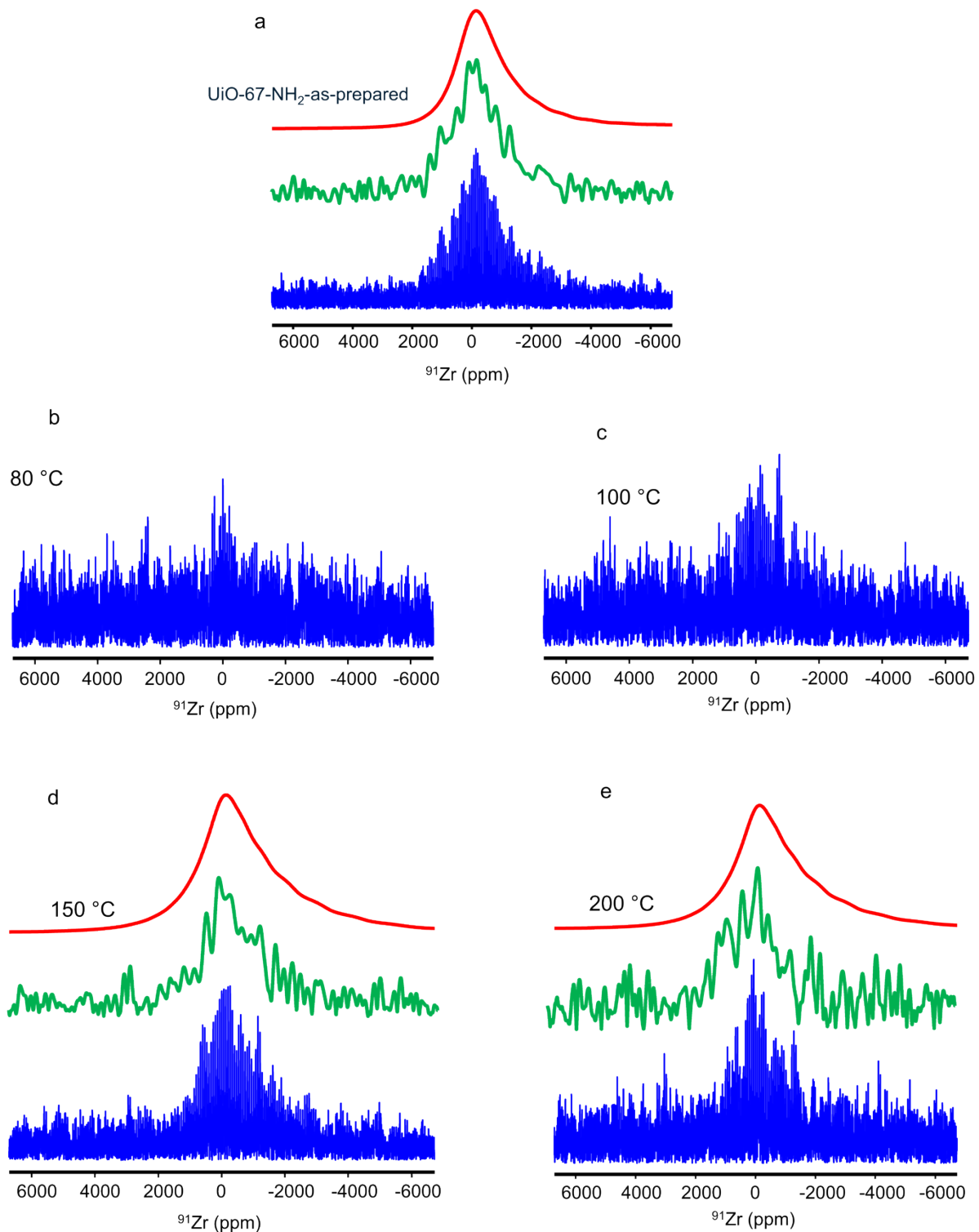


Figure S9. Experimental 1D ^{91}Zr WURST-QCPMG NMR spectra of UiO-67-NH_2 : (a) as-prepared or after steam flow treatment at (b) 80, (c) 100, (d) 150 and (e) 200 °C. The spikelet spectra in blue are obtained by the FT of the echo train and are identical to those displayed in Figures 3c and 6, whereas the envelopes in green results from the FT of the sum of the echoes. The red spectra correspond to the simulation using dmfit software.

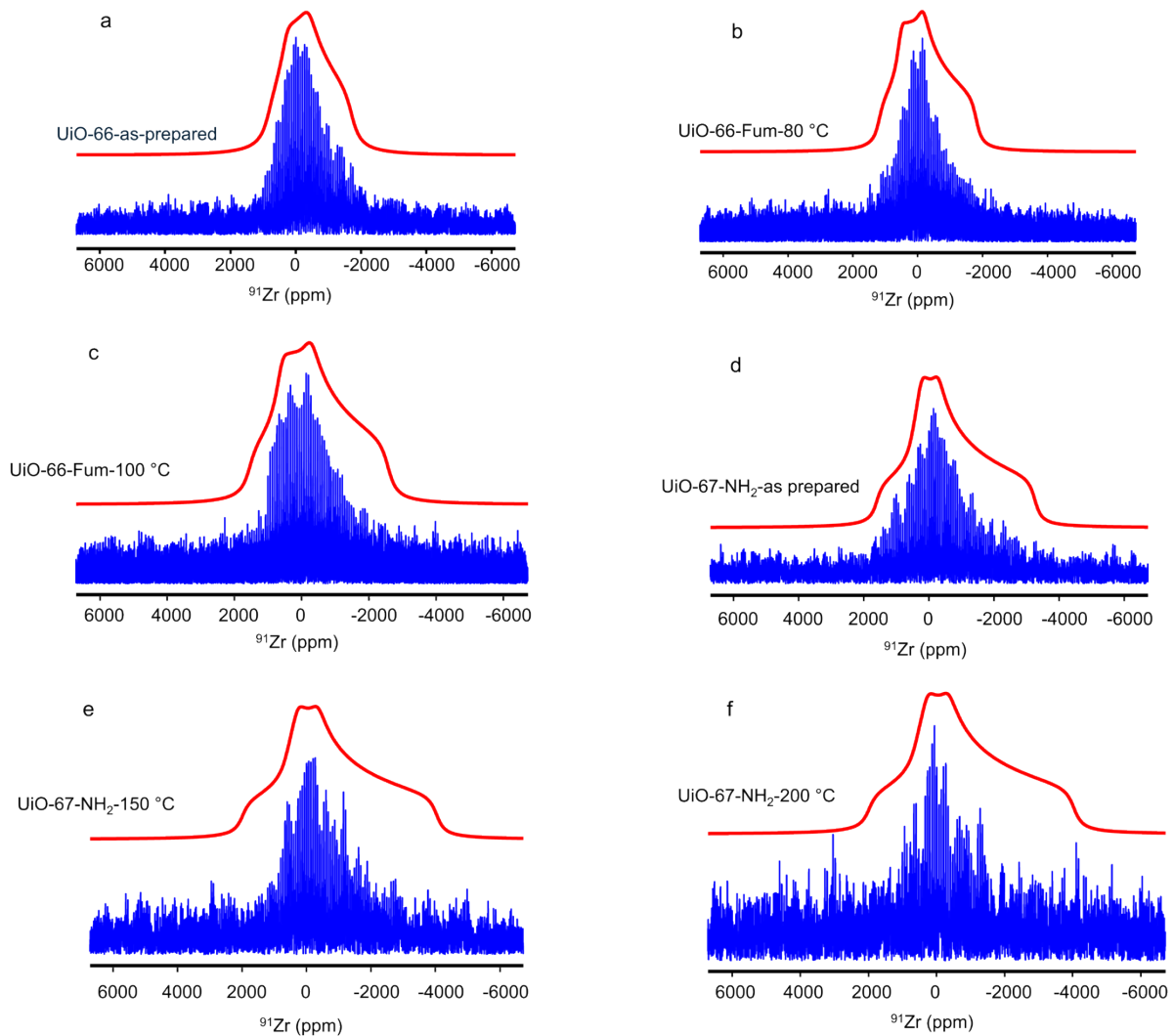


Figure S10. Experimental 1D ^{91}Zr WURST-QCPMG NMR spectra of (a) as-prepared UiO-66 , (b-c) UiO-66-Fum after steam flow at (b) 80 and (c) 100 °C and (d-f) UiO-67-NH_2 : (d) as-prepared and after steam flow at (c) 150 and (e) 200 °C. The spikelet spectra in blue are obtained by the FT of the echo train and are identical to those displayed in Figures 3 to 6. The red spectra correspond to the simulation using dmfit software and a quadrupolar lineshape for a single site, whereas Czjzek model was employed to simulate these spectra in other figures. The best-fit NMR parameters corresponding to the simulations displayed in this figure are shown in Table S3.

Table S3. Best-fit NMR parameters to simulate the experimental 1D ^{91}Zr WURST-QCPMG NMR spectra of Figure S10 using a quadrupolar lineshape of a single site.

Sample	Temperature of steam treatment (°C)	δ_{iso} (ppm)	C_Q (MHz)	η_Q
UiO-66	As-prepared	-26 (\pm 50)	16.8	0.65
UiO-66-Fum	80	120 (\pm 80)	18.0	0.70
	100	170 (\pm 50)	21.0	0.72
UiO-67-NH ₂	As-prepared	-20 (\pm 100)	22	0.85
	150	-25 (\pm 100)	24.5	0.85
	200	-25 (\pm 100)	24.5	0.85

Table S4. Calculated ^{91}Zr NMR parameters of UiO-66-Fum .

	δ_{iso} (ppm)	C_Q (MHz)	η_Q	δ_{11} (ppm)	δ_{22} (ppm)	δ_{33} (ppm)
Zr1	-45	27.3	0.7	-152	-113	130
Zr2	-48	27.2	0.8	-156	-111	123
Zr3	-48	27.4	0.7	-156	-112	125
Zr4	-45	27.3	0.7	-152	-113	130
Zr5	-48	27.2	0.8	-156	-112	123
Zr6	-48	27.4	0.8	-156	-112	124
Zr7	-45	27.3	0.7	-153	-113	130
Zr8	-48	27.2	0.8	-156	-112	123
Zr9	-47	27.4	0.8	-155	-111	125
Zr10	-45	27.3	0.7	-153	-113	130
Zr11	-48	27.5	0.7	-156	-112	124
Zr12	-46	27.2	0.7	-152	-113	128
Zr13	-48	27.5	0.7	-156	-112	124
Zr14	-48	27.2	0.8	-156	-112	123
Zr15	-46	27.5	0.7	-152	-114	129
Zr16	-46	27.2	0.7	-153	-113	128
Zr17	-45	27.5	0.7	-152	-114	129
Zr18	-48	27.4	0.7	-156	-112	125
Zr19	-48	27.6	0.7	-155	-112	125
Zr20	-45	27.5	0.7	-152	-114	130
Zr21	-46	27.2	0.7	-153	-113	128
Zr22	-48	27.5	0.8	-155	-112	124
Zr23	-46	27.2	0.7	-153	-114	128
Zr24	-46	27.5	0.7	-152	-114	129

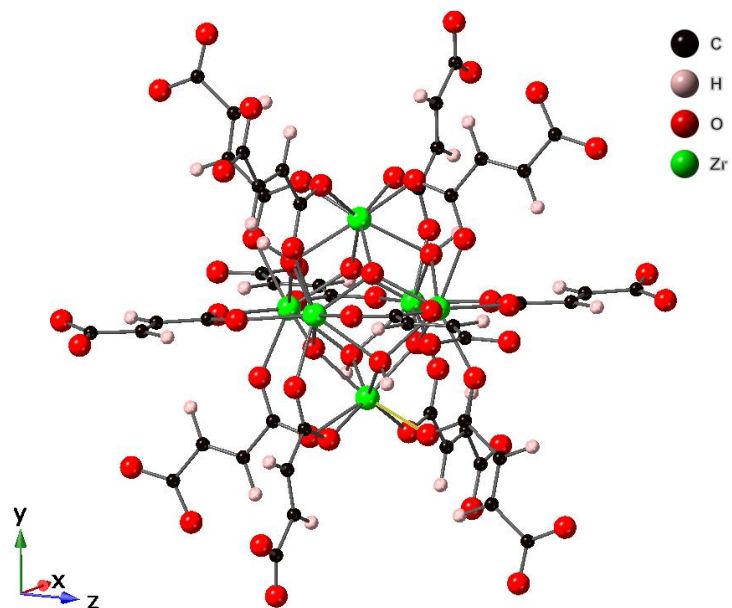


Figure S11. Atomic-level positions of UiO-66-Fum after the optimization of the structure (see main text for details).

Table S5. Calculated ^{91}Zr NMR parameters of $\text{UiO-66-Fum-H}_2\text{O}$.

	δ_{iso} (ppm)	C_Q (MHz)	η_Q	δ_{11} (ppm)	δ_{22} (ppm)	δ_{33} (ppm)
Zr1	-53	27.4	0.8	-164	-114	118
Zr2	-49	25.7	0.9	-164	-115	130
Zr3	-45	25.9	0.8	-158	-112	134
Zr4	-46	25.6	0.9	-156	-107	126
Zr5	-54	25.9	0.8	-169	-119	127
Zr6	-49	26.7	0.9	-158	-107	120
Zr7	-46	27.3	0.7	-159	-112	132
Zr8	-44	27.7	0.7	-146	-110	123
Zr9	-51	26.3	0.9	-162	-110	120
Zr10	-49	28.1	0.8	-161	-111	124
Zr11	-51	26.3	0.8	-167	-118	131
Zr12	-48	26.9	0.7	-161	-115	131
Zr13	-46	26.7	0.8	-155	-108	125
Zr14	-49	27.3	0.8	-159	-110	122
Zr15	-44	26.4	0.8	-151	-108	127
Zr16	-46	27.2	0.8	-155	-107	125
Zr17	-44	26.1	0.8	-151	-108	128
Zr18	-52	26.4	0.9	-163	-111	119
Zr19	-46	27.1	0.8	-160	-108	130
Zr20	-47	26.0	0.9	-158	-112	128
Zr21	-50	26.7	0.7	-163	-116	129
Zr22	-55	27.2	0.8	-165	-113	115
Zr23	-45	26.7	0.7	-157	-112	134
Zr24	-45	27.4	0.8	-155	-107	126

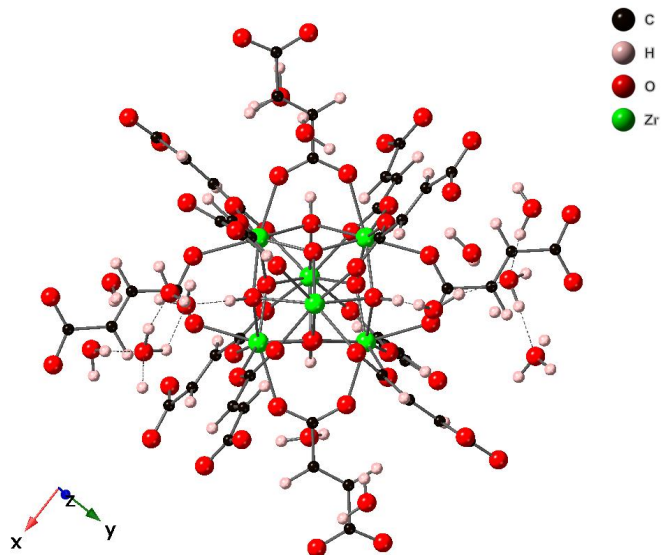


Figure S12. Atomic-level positions of $\text{UiO-66-Fum-H}_2\text{O}$ after the optimization of the structure (see main text for details).

Table S6. Calculated ^{91}Zr NMR parameters of UiO-67-NH_2 .

	δ_{iso} (ppm)	C_Q (MHz)	η_Q	δ_{11} (ppm)	δ_{22} (ppm)	δ_{33} (ppm)
Zr1	-56	29.4	0.6	-170	-128	129
Zr2	-56	29.1	0.6	-170	-128	131
Zr3	-56	26.7	0.8	-165	-127	126
Zr4	-54	25.9	0.8	-165	-127	131
Zr5	-55	25.8	0.8	-164	-126	126
Zr6	-55	26.8	0.7	-165	-128	128

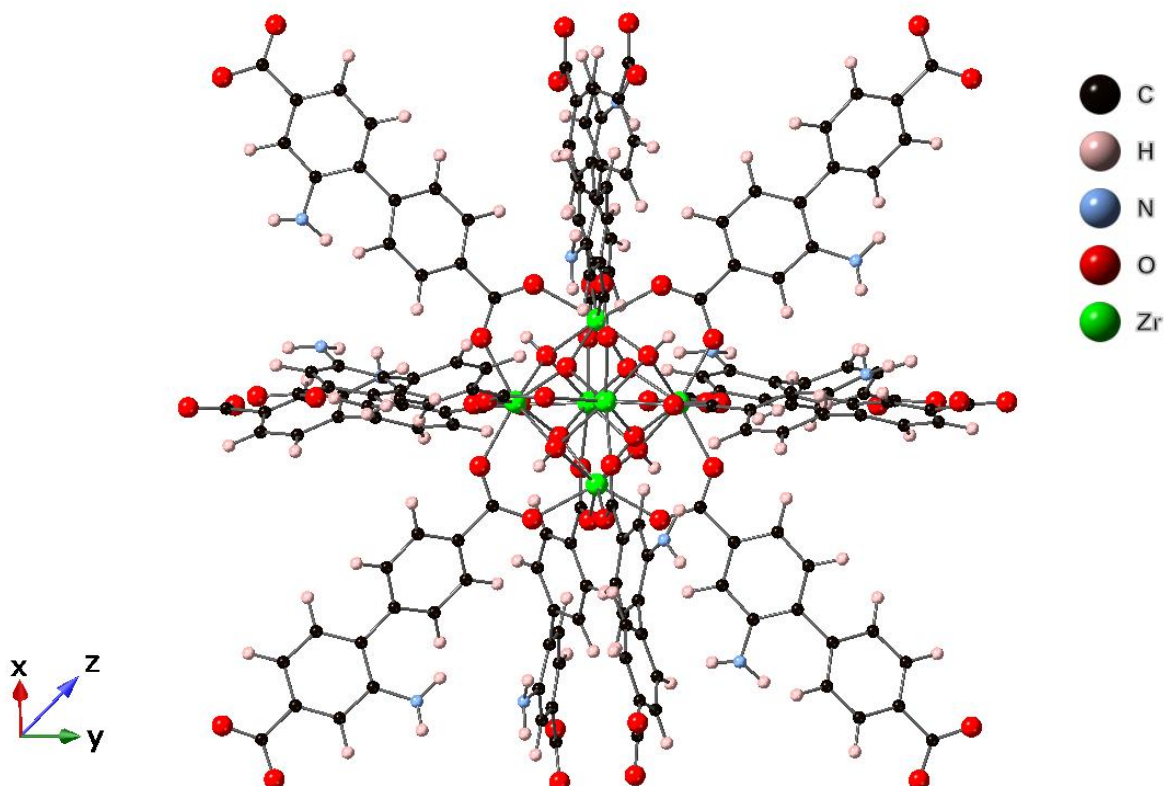


Figure S13. Atomic-level positions of UiO-67-NH_2 after the optimization of the structure (see main text for details).

Table S7. List of reference structures used to estimate the precision of calculated $\delta_{\text{iso}}(^{91}\text{Zr})$ and $C_Q(^{91}\text{Zr})$ values by comparing experimental and DFT calculated NMR parameters

	ICSD Code	σ_{iso} calc. (ppm)	δ_{iso} exp. (ppm)	$ C_Q $ calc. (MHz)	C_Q exp. (MHz)
ZrO ₂	62993	1832	96 ⁶	19.4	23.4 ⁶
BaZrO ₃	97459	1621	316 ⁶	-	-
ZrSiO ₄	71943	1983	-74 ⁶	20.8	20.5 ⁶
SrZrO ₃	650	1659	290 ⁷	6.3	4.3 ⁸
MIL140A	CCDC 905026	1889	100 ⁹	35.4	35.0 ⁹

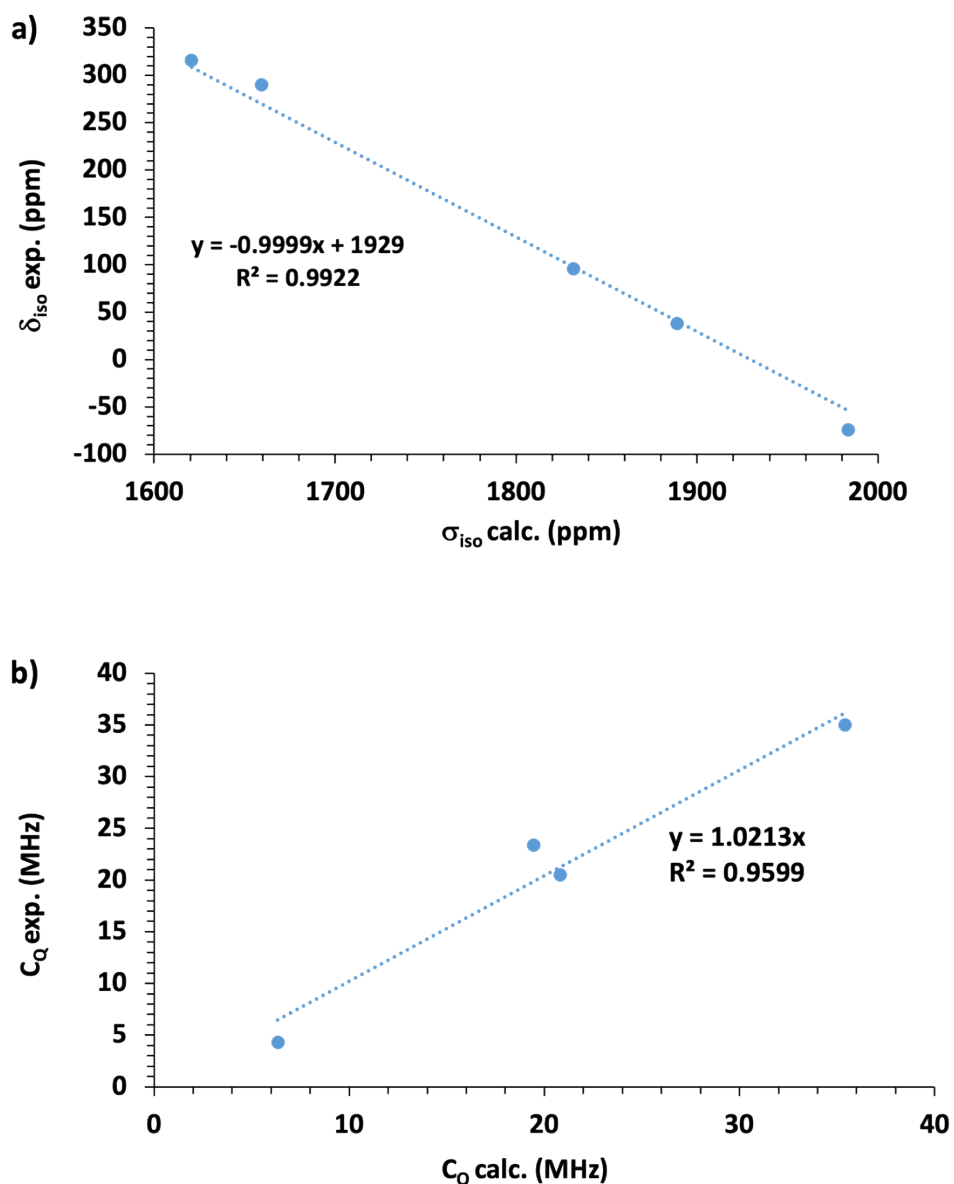


Figure S14. (a) Experimental $\delta_{\text{iso}}(^{91}\text{Zr})$ values (in ppm) vs calculated σ_{iso} (b) Experimental C_Q values (in MHz) vs calculated ones

References

- (1) Oien, S.; Wragg, D.; Reinsch, H.; Svelle, S.; Bordiga, S.; Lamberti, C.; Lillerud, K. P. Detailed Structure Analysis of Atomic Positions and Defects in Zirconium Metal-Organic Frameworks. *Cryst. Growth Des.* **2014**, *14* (11), 5370-5372. DOI: 10.1021/cg501386j.
- (2) Furukawa, H.; Gándara, F.; Zhang, Y. B.; Jiang, J. C.; Queen, W. L.; Hudson, M. R.; Yaghi, O. M. Water Adsorption in Porous Metal-Organic Frameworks and Related Materials. *J. Am. Chem. Soc.* **2014**, *136* (11), 4369-4381. DOI: 10.1021/ja500330a.
- (3) Goodenough, I.; Devulapalli, V. S. D.; Xu, W.; Boyanich, M. C.; Luo, T.-Y.; De Souza, M.; Richard, M.; Rosi, N. L.; Borguet, E. Interplay between Intrinsic Thermal Stability and Expansion Properties of Functionalized UiO-67 Metal–Organic Frameworks. *Chem. Mater.* **2021**, *33* (3), 910-920. DOI: 10.1021/acs.chemmater.0c03889.
- (4) Valenzano, L.; Civalleri, B.; Chavan, S.; Bordiga, S.; Nilsen, M. H.; Jakobsen, S.; Lillerud, K. P.; Lamberti, C. Disclosing the complex structure of UiO-66 metal organic framework: A synergic combination of experiment and theory. *Chem. Mater.* **2011**, *23* (7), 1700-1718. DOI: 10.1021/cm1022882 Scopus.
- (5) Giovine, R.; Pourpoint, F.; Duval, S.; Lafon, O.; Amoureux, J. P.; Loiseau, T.; Volkringer, C. The Surprising Stability of Cu₃(btc)₂ Metal-Organic Framework under Steam Flow at High Temperature. *Cryst. Growth Des.* **2018**, *18* (11), 6681-6693. DOI: 10.1021/acs.cgd.8b00931.
- (6) Lapina, O. B.; Khabibulin, D. F.; Terskikh, V. V. Multinuclear NMR study of silica fiberglass modified with zirconia. *Solid State Nucl. Magn. Reson.* **2011**, *39* (3-4), 47-57. DOI: 10.1016/j.ssnmr.2010.12.002.
- (7) Czernek, J.; Kobera, L.; Havlák, L.; Czerneková, V.; Rohlíček, J.; Bárta, J.; Brus, J. Probing the ⁹¹Zr NMR parameters in the solid state by a combination of DFT calculations and experiments. *Chem. Phys. Lett.* **2020**, *738*, 136855. DOI: 10.1016/j.cplett.2019.136855.
- (8) Rebaza, A.; Navarro, A.; Taylor, M.; Errico, A.; Cottenier, S. Hyperfine properties at Zr sites of Zr-based compounds. A DFT FP-LAPW and GIPAW study. *Phys. B- Condensed Matter* **2023**, *657*, 414757. DOI: 10.1016/j.physb.2023.414757.
- (9) He, P.; Lucier, B. E. G.; Terskikh, V. V.; Shi, Q.; Dong, J. X.; Chu, Y. Y.; Zheng, A. M.; Sutrisno, A.; Huang, Y. N. Spies Within Metal-Organic Frameworks: Investigating Metal Centers Using Solid-State NMR. *J. Phys. Chem. C* **2014**, *118* (41), 23728-23744. DOI: 10.1021/jp5063868.